

# Low-Temperature Synthesis of Amorphous FeP<sub>2</sub> and Its Use as Anodes for Li Ion Batteries

Justin W. Hall,<sup>†</sup> Nellymar Membreno,<sup>†</sup> Jing Wu,<sup>†</sup> Hugo Celio,<sup>‡</sup> Richard A. Jones,<sup>\*,†</sup> and Keith J. Stevenson<sup>\*,†</sup>

<sup>†</sup>Department of Chemistry and Biochemistry, University of Texas at Austin, Austin, Texas 78712, United States

<sup>‡</sup>Texas Materials Institute, University of Texas at Austin, Austin, Texas 78712, United States

## Supporting Information

**ABSTRACT:** The reaction of Fe(N(SiMe<sub>3</sub>)<sub>2</sub>)<sub>3</sub> with PH<sub>3</sub> in THF at 100 °C gives amorphous FeP<sub>2</sub> in high yield. As an anode material in a Li ion battery, this material shows remarkable performance toward electrochemical lithiation/delithiation, with gravimetric discharge and charge capacities of 1258 and 766 mA h g<sup>-1</sup>, respectively, translating to 61% reversibility on the first cycle and a discharge capacity of 906 mA h g<sup>-1</sup> after 10 cycles. This translates to 66% retention of the theoretical full conversion capacity of FeP<sub>2</sub> (1365 mA h g<sup>-1</sup>).

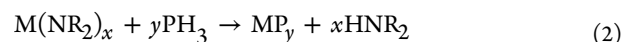
Lithium ion batteries are currently used in small appliances such as cell phones and laptop computers and are the most promising power source for plug-in hybrid electric vehicles (PHEVs) and electric vehicles (EVs).<sup>1a,b</sup> These modes of transportation have the potential to reduce CO<sub>2</sub> emissions greatly and to reduce our dependence on foreign oil. Lithium ion battery cathode materials that meet many of the requirements for utilization in PHEVs and EVs, including high charge and discharge rates, have been discovered.<sup>1c,d</sup> Lithiated graphite is currently the most widely used anode, although considerable improvements in safety, cost, and weight are sought as well as materials with higher capacity and higher power in order to realize the full potential of PHEVs and EVs.<sup>2–4</sup>

Anode materials based on inexpensive transition-metal phosphides (TMPs) offer great promise for lithium ion batteries because of their exceptionally high gravimetric storage capacities relative to conventional lithium ion carbon anode materials. However, lithium ion-coupled charge transfer reactions in TMPs induce large irreversible volume changes in excess of 300% due to the formation of Li<sub>x</sub>M, Li<sub>x</sub>P, and M<sup>0</sup> phases. This can facilitate failure processes including aggregation and pulverization as well as loss of electrical contact between the active material and the current collector (support). While such a drastic volume change cannot be alleviated completely, the magnitude of the volume change can be reduced by the use of TMPs with a more optimized nanostructure and porous or layered architecture.<sup>5–7</sup> Of the TMP materials studied to date, FeP, FeP<sub>2</sub>, and FeP<sub>4</sub> are attractive because they are based on inexpensive iron. The theoretical full conversion capacities of FeP, FeP<sub>2</sub>, and FeP<sub>4</sub> are 926, 1365, and 1789 mA h g<sup>-1</sup>, respectively, all of which are

considerably greater than that of the traditional graphite anode (372 mA h g<sup>-1</sup>).<sup>8,9</sup>

Current methods of preparing nanosized particles of TMPs typically employ arrested precipitation or solvothermal routes, both of which require relatively high temperatures. For the late transition metals, pioneering studies by Brock<sup>10</sup> and Schaak<sup>11</sup> on the synthesis of nanosized TMPs have been focused on the use of trioctylphosphine (TOP) and trioctylphosphine oxide (TOPO) at temperatures generally in the range 200–300 °C.<sup>12–18</sup> In addition, Brock<sup>10h</sup> has also demonstrated that desilylation could be used to produce FeP nanoparticles at 240–300 °C. These high-temperature routes to TMPs in most cases provide the most thermodynamically stable, well-known crystalline phase of the material. In contrast, we have discovered that  $\sigma$ -bonded metal alkyls<sup>19</sup> or dialkylamide derivatives<sup>20</sup> of the d-block transition metals react readily with PH<sub>3</sub> at room temperature or slightly elevated temperatures to give kinetically stabilized amorphous or nanocrystalline phases of TMPs in high yields.<sup>21</sup> We have to date prepared amorphous phosphides of Ti, Mo, Fe, Mn, and Ni by this method. The phosphides of Ti, Mo, Mn, and Ni, will be reported separately.

Since the main byproduct from these reactions (eqs 1 and 2) are alkanes or secondary amines, this process represents a relatively clean and simple method of producing these materials.



Thus, the reaction of the mononuclear Fe amide Fe(N(SiMe<sub>3</sub>)<sub>2</sub>)<sub>3</sub> with PH<sub>3</sub> in THF solution produces a black, air-sensitive powder.<sup>22,23</sup> Preliminary scanning electron microscopy (SEM) data revealed that the product is an aggregate material with particles ranging from 10 to 50 nm in size (Figure 1), and no diffraction peaks were observed in the powder X-ray diffraction pattern. Microanalytical data established the Fe:P ratio as 1:1.99. Peaks that could be assigned to residual P–H or C–H moieties were also absent from the IR spectrum. The surface area, as measured by multipoint Brunauer–Emmett–Teller analysis with N<sub>2</sub>, was 140 m<sup>2</sup>/g. This material, that did

Received: February 5, 2012

Published: March 15, 2012

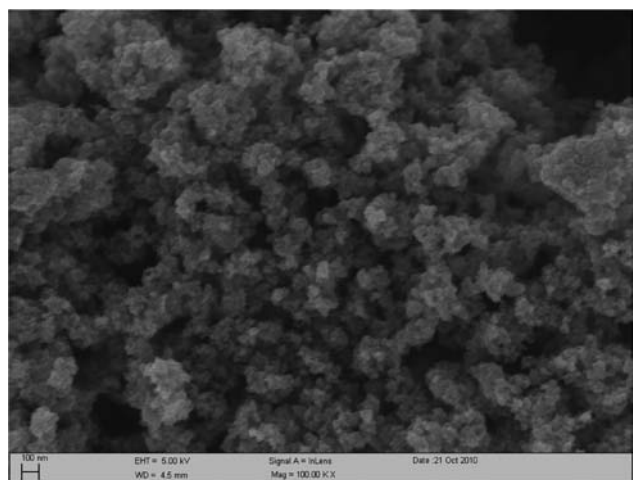


**Figure 1.** SEM image of amorphous  $\text{FeP}_2$  synthesized at low temperature.

not undergo high-temperature annealing, showed significant promise as an anode material.

Preliminary electrochemical studies showed excellent performance toward lithiation/delithiation (Figure 2), with

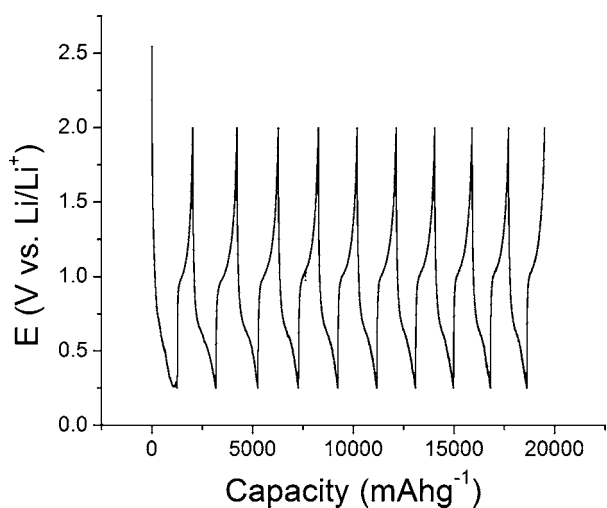


**Figure 2.** Discharge/charge plot of amorphous  $\text{FeP}_2$  over 10 cycles at 0.1 C.

gravimetric discharge and charge capacities of 1258 and 766  $\text{mA h g}^{-1}$ , translating to 61% reversibility on the first cycle (Figure 3). The initial capacity of our material compares favorably with that of crystalline  $\text{FeP}_2$  prepared via conventional high-temperature routes.<sup>9a,c</sup> Boyanov et al.<sup>9a</sup> reported that  $\text{FeP}_2$  prepared by heating powders of the elements to 973 K for 5 days has an initial capacity of 1000  $\text{mA h g}^{-1}$  and a capacity loss of 34% during the first cycle, leading to a reversible capacity of 653  $\text{mA h g}^{-1}$ . A sustained cyclability of 300  $\text{mA h g}^{-1}$  could be obtained only by limiting the potential window. Ouvrard and co-workers<sup>9c</sup> also reported that  $\text{FeP}_2$  prepared using the elements in a tin flux method had an initial capacity of 1365  $\text{mA h g}^{-1}$ , but they did not indicate whether significant capacity was retained upon continuous cycling.

For our amorphous  $\text{FeP}_2$ , some of the irreversible capacity loss on the first cycle is associated with the irreversible formation of a solid electrolyte interphase (SEI) layer, as is

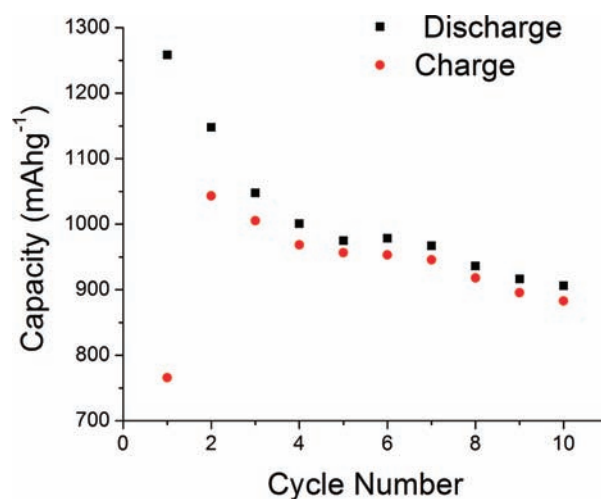
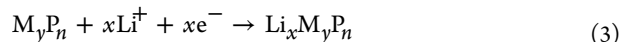


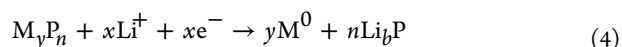
**Figure 3.** Discharge and charge capacities for the first 10 cycles of amorphous  $\text{FeP}_2$  at 0.1 C.

common for anode materials cycled below 1 V vs  $\text{Li}/\text{Li}^+$ . Although our material demonstrated gradual capacity loss, the cyclability is superior to that in any previous work presented for  $\text{FeP}_2$ , with 66% retention of the theoretical capacity on the 10th cycle ( $906 \text{ mA h g}^{-1}$ ).<sup>24</sup> We attribute our better retention to both the amorphous and nanostructural nature of our material, which alleviate the severe mechanical strain upon lithiation/delithiation. In a comparative study between crystalline and amorphous  $\text{MnO}_x$  nanoparticles, Guo et al.<sup>5b</sup> showed not only that the cycling stability was improved but also that subsequent lithiation potentials (after the first cycle) changed only slightly, confirming the enhanced structural stability of the amorphous material.

Depending on the transition metal, TMPs can be categorized with two lithiation mechanisms:  $\text{Li}^+$  insertion or intercalation,



or  $\text{Li}^+$  conversion or alloying,



where M is the transition metal and b is the oxidation state of P.

An incremental capacitance plot analogous to slow-scan cyclic voltammetry (SSCV) exhibited a reversible lithiation potential centered at 0.56 V vs  $\text{Li}/\text{Li}^+$  on the first discharge and thereafter remained at around 0.65 V (Figure 4). Delithiation takes place at 1.00 V vs  $\text{Li}/\text{Li}^+$ . From analysis of this plot, it appears that the charge storage mechanism involves contributions from the  $\text{Li}^+$  insertion/deinsertion reaction and a possible conversion process (consistent with that reported previously).<sup>9a</sup> However, we do not see evidence for an initial direct conversion of the  $\text{FeP}_2$  starting material to form  $\text{Li}_3\text{P}$  and  $\text{Fe}^0$  in the first discharge. In our amorphous  $\text{FeP}_2$  material, the lithiation/delithiation is highly reversible with high capacity retention.

More studies are underway to elucidate the reaction mechanism with lithium. As reported previously, the lithiation/delithiation process in crystalline TMPs is complex, showing distinct electrochemical features and charge/discharge plateaus consistent with the existence of different structures/phases.<sup>9a</sup>

Precaution must be taken with the amorphous  $\text{FeP}_2$  produced by our low-temperature route, as even minimal air

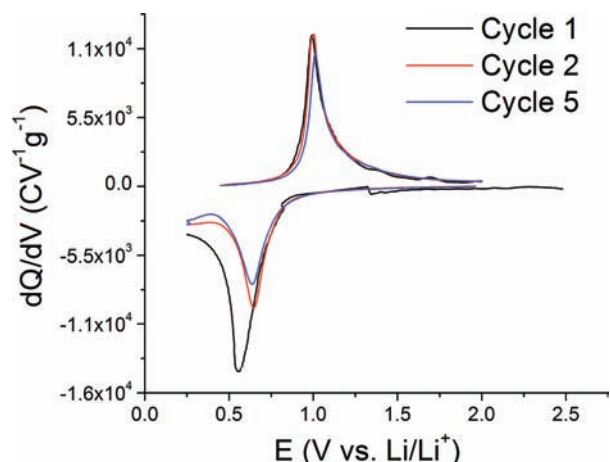


**Figure 4.** Incremental capacitance plots of the first (black), second (red), and fifth (blue) cycles of amorphous  $\text{FeP}_2$ .

exposure is detrimental to the electrochemical properties of the material. Following brief exposure, a drastic reduction of the initial discharge capacity to  $130 \text{ mA h g}^{-1}$  along with an absence of voltage plateau features on the discharge/charge plot indicated that the electrode became inactive (Figure S1 in the Supporting Information). Consequently, amorphous  $\text{FeP}_2$  was handled in an inert environment prior to fabrication of the coin cell in order to determine its characteristic electrochemical properties.

One major factor for exploiting these phosphide-based materials in future applications lies in controlling the kinetics of lithium insertion, thereby lowering the charge/discharge polarization voltage, which is currently responsible for the still poor energy performance of anode (negative) electrodes. Controlling the geometrical orientation and alignment of TMPs and/or the coating of TMP nanostructures are other compelling strategies for suppressing volume changes and preventing degradation processes.<sup>25</sup> Our new low-temperature synthetic strategy for the preparation of kinetically stabilized TMPs may allow us to develop suitable design criteria and guiding principles that allow for control over the morphology and composition and thus help us to discover electrode architectures with enhanced mass and charge transport, electron and ion conductivity, and electron transfer kinetics.<sup>26,27</sup>

## ■ ASSOCIATED CONTENT

### Supporting Information

Detailed synthetic and characterization procedures and data. This material is available free of charge via the Internet at <http://pubs.acs.org>.

## ■ AUTHOR INFORMATION

### Corresponding Author

rajones@mail.utexas.edu; stvenson@cm.utexas.edu

### Notes

The authors declare no competing financial interest.

## ■ ACKNOWLEDGMENTS

We thank the Welch Foundation (Grants F-816 and F-1529) and the Norman Hackerman Advanced Research Program (003658-0030-2009) for financial support.

## ■ REFERENCES

- (1) (a) Karden, E.; Ploumen, S.; Fricke, B.; Miller, T.; Snyder, K. J. *Power Sources* **2007**, *168*, 2–11. (b) Kennedy, B.; Patterson, D.; Camilleri, S. J. *Power Sources* **2000**, *90*, 156–162. (c) Scrosati, B.; Garche, J. J. *Power Sources* **2010**, *195*, 2419. (d) Kang, B.; Ceder, G. *Nature* **2009**, *458*, 190.
- (2) Biensan, P.; Simon, B.; Pere, J. P.; de Guibert, A.; Broussely, M.; Bodet, J. M.; Pertion, F. J. *Power Sources* **1999**, *81*, 906.
- (3) Choi, N.-S.; Profatlova, I. A.; Kim, S.-S.; Song, E.-H. *Thermochim. Acta* **2008**, *480*, 10–14.
- (4) Haxel, G. B.; Hedrick, J. B.; Orris, G. J.; *Rare Earth Elements—Critical Resources for High Technology*; Fact Sheet 087–02; U.S. Geological Survey: Reston, VA, 2002.
- (5) (a) Bruce, P. G.; Scrosati, B.; Tarascon, J.-M. *Angew. Chem., Int. Ed.* **2008**, *47*, 2930. (b) Guo, J.; Liu, Q.; Wang, C.; Zachariah, M. R. *Adv. Funct. Mater.* **2011**, *22*, 803–811.
- (6) Guo, Y.-G.; Hu, J.-S.; Wan, L.-J. *Adv. Mater.* **2008**, *20*, 2878–2887.
- (7) Wang, Y.; Cao, G. *Adv. Mater.* **2008**, *20*, 2251–2269.
- (8) (a) Gillot, F.; Bichat, M. P.; Favier, F.; Morcrette, M.; Doublet, M. L.; Monconduit, L. *Electrochim. Acta* **2004**, *49*, 2325–2332. (b) Pralong, V.; Souza, D. C. S.; Leung, K. T.; Nazar, L. F. *Electrochem. Commun.* **2002**, *4*, 516–520. (c) Souza, D. C. S.; Pralong, V.; Jacobson, A. J.; Nazar, L. F. *Science* **2002**, *296*, 2012–2015. (d) Doublet, M.-L.; Lemoigno, F.; Gillot, F.; Monconduit, L. *Chem. Mater.* **2002**, *14*, 4126–4133. (e) Bichat, M.-P.; Gillot, F.; Monconduit, L.; Favier, F.; Morcrette, M.; Lemoigno, F.; Doublet, M.-L. *Chem. Mater.* **2004**, *16*, 1002–1013. (f) Gillot, F.; Monconduit, L.; Doublet, M.-L. *Chem. Mater.* **2005**, *17*, 5817–5823. (g) Bichat, M.-P.; Pascal, J.-L.; Gillot, F.; Favier, F. *Chem. Mater.* **2005**, *17*, 6761–6771. (h) Boyanov, S.; Bernardi, J.; Gillot, F.; Dupont, L.; Womes, M.; Tarascon, J.-M.; Monconduit, L.; Doublet, M.-L. *Chem. Mater.* **2006**, *18*, 3531–3538. (i) Gillot, F.; Menetrier, M.; Bekaert, E.; Dupont, L.; Morcrette, M.; Monconduit, L.; Tarascon, J. M. *J. Power Sources* **2007**, *172*, 877–885. (j) Boyanov, S.; Annou, K.; Villeveille, C.; Pelosi, M.; Zitoun, D.; Monconduit, L. *Ionics* **2008**, *14*, 183–190. (k) Villeveille, C.; Robert, F.; Taberna, P. L.; Bazin, L.; Simon, P.; Monconduit, L. *J. Mater. Chem.* **2008**, *18*, 5956–5960. (l) Kim, M. G.; Lee, S.; Cho, J. J. *Electrochem. Soc.* **2009**, *156*, A89–A94. (m) Boyanov, S.; Bernardi, J.; Bekaert, E.; Menetrier, M.; Doublet, M.-L.; Monconduit, L. *Chem. Mater.* **2009**, *21*, 298–308. (n) Kim, M. G.; Cho, J. J. *Electrochem. Soc.* **2009**, *156*, A277–A282. (o) Mauchamp, V.; Moreau, P.; Monconduit, L.; Doublet, M.; Boucher, F.; Ouard, G. *J. Phys. Chem. C* **2007**, *111*, 3996–4002. (p) Xiang, J. Y.; Wang, X. L.; Zhong, J.; Zhang, D.; Tu, J. P. *J. Power Sources* **2011**, *196*, 379–385. (q) Xiang, J. Y.; Wang, X. L.; Xia, X. H.; Zhong, J.; Tu, J. P. *J. Alloys Compd.* **2011**, *509*, 157–160.
- (9) (a) Boyanov, S.; Zithoun, D.; Menetrier, M.; Jumas, J. C.; Womes, M.; Monconduit, L. *J. Phys. Chem. C* **2009**, *113*, 21441–21452. (b) Boyanov, S.; Womes, M.; Jumas, J. C.; Monconduit, L. *Hyperfine Interact.* **2008**, *187*, 57–69. (c) Silva, D. C. C.; Crosnier, O.; Ouvrard, G.; Greedan, J.; Safa-Sefat, A.; Nazar, L. F. *Electrochem. Solid State Lett.* **2003**, *6*, A162–A165.
- (10) (a) Brock, S. L.; Senevirathne, K. *J. Solid State Chem.* **2008**, *181*, 1552–1559. (b) Stamm, K. L.; Brock, S. L. *J. Alloys Compd.* **2008**, *453*, 476–481. (c) Senevirathne, K.; Burns, A. W.; Bussell, M. E.; Brock, S. L. *Adv. Funct. Mater.* **2007**, *17*, 3933–3939. (d) Gregg, K. A.; Perera, S. C.; Lawes, G.; Shinozaki, S.; Brock, S. L. *Chem. Mater.* **2006**, *18*, 879–886. (e) Somaskandan, K.; Tsoi, G. M.; Wenger, L. E.; Brock, S. L. *Chem. Mater.* **2005**, *17*, 1190–1198. (f) Aitken, J. A.; Ganzha-Hazen, V.; Brock, S. L. *J. Solid State Chem.* **2005**, *178*, 970–975. (g) Perera, S. C.; Brock, S. L. *Mater. Res. Soc. Symp. Proc.* **2003**, *755*, DD5.91–DD6.12.6. (h) Perera, S. C.; Fodor, P. S.; Tsoi, G. M.; Wenger, L. E.; Brock, S. L. *Chem. Mater.* **2003**, *15*, 4034–4038. (i) Perera, S. C.; Tsoi, G.; Wenger, L. E.; Brock, S. L. *J. Am. Chem. Soc.* **2003**, *125*, 13960–13961. (j) Stamm, K. L.; Garno, J. C.; Liu, G.-Y.; Brock, S. L. *J. Am. Chem. Soc.* **2003**, *125*, 4038–4039. (k) Muthuswamy, E.; Brock, S. L. *J. Am. Chem. Soc.* **2010**, *132*, 15849–15851. (l) Muthuswamy, E.; Brock, S. L. *Chem. Commun.* **2011**, *47*, 12334–12336.

(11) (a) Henkes, A. E.; Schaak, R. E. *Inorg. Chem.* **2008**, *47*, 671–677. (b) Henkes, A. E.; Vasquez, Y.; Schaak, R. E. *J. Am. Chem. Soc.* **2007**, *129*, 1896–1897. (c) Henkes, A. E.; Schaak, R. E. *Chem. Mater.* **2007**, *19*, 4234–4242.

(12) Qian, C.; Kim, F.; Ma, L.; Tsui, F.; Yang, P.; Liu, J. *J. Am. Chem. Soc.* **2004**, *126*, 1195–1198.

(13) Wang, M.; McDonald, R.; Mar, A. *Inorg. Chem.* **2000**, *39*, 4936–4941.

(14) (a) Kleinke, H.; Franzen, H. F. *J. Solid State Chem.* **1997**, *131*, 379–386. (b) Kleinke, H.; Franzen, H. F. *J. Am. Chem. Soc.* **1997**, *119*, 12824–12830.

(15) Chen, L.; Huang, M.; Gu, Y.; Shi, L.; Yang, Z.; Qian, Y. *Mater. Lett.* **2004**, *58*, 3337–3339.

(16) Liu, S.; Qian, Y.; Xu, L. *Solid State Commun.* **2009**, *149*, 438–440.

(17) Barry, B. M.; Gillan, E. G. *Chem. Mater.* **2008**, *20*, 2618–2620.

(18) George, P. P.; Pol, V. G.; Gedanken, A. *J. Nanopart. Res.* **2007**, *9*, 1187–1193.

(19) (a) Davidson, P. J.; Lappert, M. F.; Pearce, R. *Chem. Rev.* **1976**, *76*, 219–242. (b) Schrock, R. R.; Parshall, G. W. *Chem. Rev.* **1976**, *76*, 243–268.

(20) Lappert, M. F.; Power, P. P.; Protchenko, A.; Seeber, A. *Metal Amide Chemistry*; Wiley: Chichester, U.K., 2008; Chapter 6, pp 149–204.

(21) Literature from the 19th and early 20th centuries contains evidence that  $\text{PH}_3$  reacts with salts of Cr, U, Mn, Ni, Co, and Fe to form metal phosphides. However, these materials were poorly characterized, and these reactions do not appear to have been investigated in the modern era. For example, see: *Gmelins Handb. Anorg. Chem., Part C* **1965**, *16*, 45–47.

(22) **Caution:** Phosphine is a highly poisonous and reactive gas. All operations must be performed by highly trained personnel under rigorous exclusion of air.

(23) Alyea, E. C.; Bradley, D. C.; Copperthwaite, R. G. *Dalton Trans.* **1972**, 1580–1584.

(24) Cyclability is defined as the Coulombic efficiency between lithation and delithation. In specific terms, the Coulombic efficiency of a battery is the ratio of the integrated charge associated with charging to the charge that can be extracted from the battery during discharging. The losses that reduce the Coulombic efficiency are primarily due to the loss of charge via secondary reactions, such as electrolysis of the solvent or other surface redox reactions in the battery.

(25) Qian, C.; Kim, F.; Ma, L.; Tsui, F.; Yang, P.; Liu, J. *J. Am. Chem. Soc.* **2004**, *126*, 1195–1198.

(26) Balaya, P.; Bhattacharyya, A. J.; Jamnik, J.; Zhukovskii, Yu. F.; Kotomin, E. A.; Maier, J. *J. Power Sources* **2006**, *159*, 171–178.

(27) Maier, J. *J. Power Sources* **2007**, *174*, S69–S74.